Available online at www.sciencedirect.com
ScienceDirect
Journal of Molecular Graphics and Modelling 25 (2007) 856–869
Journal of Molecular Graphics and Modelling
www.elsevier.com/locate/JMGM

Application of the independent molecule model to elucidate the dynamics of structure I methane hydrate

Shuzo Yoshioki *

Yatsushiro National College of Technology, Yatsushiro 866-8501, Japan

Received 18 April 2006; received in revised form 16 August 2006; accepted 22 August 2006
Available online 3 September 2006

Abstract

Raman spectroscopy has exhibited the C–H stretch (A_1 mode) frequency ν_1 of hydrated methanes at 2915 cm^{-1} for the 5^{12} cage and 2905 cm^{-1} for the $5^{12}6^2$ cage. These values are lower than the frequency of 2916.5 cm^{-1} in gaseous methane. In this paper, we theoretically examine the Raman spectra observed in methane hydrate by normal mode analysis using the independent molecule model. By a breakdown of the symmetry, the four frequencies in modes A_1, E, T_2 and T_2 observed in gaseous methane are separated into nine frequencies in the hydrate. It is necessary to consider the anharmonic potential energy within methane and hydrogen bonding between methane hydrogen and water oxygen in order to get a result in qualitative agreement with experiment. The frequency in the $5^{12}6^2$ cage is shifted downward in comparison to the one in 5^{12}, and the frequencies in the both cages are also shifted downward compared with the frequencies in gas. Calculations are also reported for the isotopic methane (CD_4, $^{13}CH_4$) hydrates.

Keywords: Methane hydrate; Dynamics; Vibrational frequency; Independent molecule model; Symmetry coordinate; Raman spectrum; Hydrogen bond; Thermal ellipsoid

1. Introduction

Methane hydrates have attracted considerable interest in regard to natural gas as a fuel [1]. These hydrates are inclusion compounds consisting of water surrounding small guest molecules of methane. The waters form ice-like hydrogen bonded cages. Clathrate hydrates, which include methane hydrate, are known to have different structures depending on the size of the guest molecules. They are structures I and II, and the hexagonal structure H [2–4].

The methane hydrates analysed in this paper form structure I. The unit cell of structure I contains eight water cages, six tetracaidecahedra (formed by 12 pentagons and 2 hexagons designated $5^{12}6^2$, hereinafter referred to as the large cage) and two dodecahedra (formed by 12 pentagons designated 5^{12}, referred to as the small cage). Raman spectra show that a methane molecule in the respective cages undergoes C–H stretching vibrations [5,6].

The main purpose of this paper is to use the independent molecule model (independent MM) to elucidate the dynamical vibrations of a methane as a guest molecule in small and large cages. The independent MM is a method developed to elucidate dynamical characters of a system consisting of multi-molecules. So far the model has been applied to systems comprised of a protein surrounded by water molecules [7], as well as water hexamers [8], and heptamers and octamers [9]. This paper is our first application to a system composed of methanes and water molecules.

In Section 2, the method of how to use the independent MM is described. The results are given in Section 3. Discussion and conclusion are given in Section 4. Finally, the Appendix presents the expressions of harmonic and cubic anharmonic potential energies within methane, and the methods necessary to do normal mode analysis.

2. Methods

2.1. Variables in the independent molecule model

This model was devised to elucidate the dynamical structure of internal motions and rigid-body motions of each molecule in a multi-molecule system. The essential point of the independent MM is to separate the motions of each molecule in the system into the rigid-body motion (with six degrees of freedom) and

* Tel.: +81 965 53 1309; fax: +81 965 53 1319.
E-mail address: yoshioki@as.yatsushiro-nct.ac.jp.

1093-3263/$ – see front matter
doi:10.1016/j.jmgm.2006.08.007

the internal motions. The variables describing movements as a rigid body are the same for each type of molecule in a multi-molecule system: a translational vector and Eulerian angles specifying position and orientation of each molecule. On the other hand, the variables describing internal movements within a molecule are different according to its chemical structure. Thus, if we consider a protein in water, the internal variables of the protein are the dihedral angles at rotatable bonds, whereas, for water molecules, two bond lengths and the bond angle in a water were chosen in earlier papers [7–9]. For methane, four bond lengths and six bond angles within a methane are chosen.

In Fig. 1, the independent variables in the independent MM are depicted. The S-system is a fixed laboratory coordinate system. Each molecule moves freely as a rigid-body. The position and orientation of each molecule with respect to the S-system is specified by a translational vector $t = (t_1, t_2, t_3)$ and Eulerian angles (τ_1, τ_2, τ_3). Three internal variables in the kth water molecule are specified by two bond lengths (ρw_1^k for the O–H_1 distance and ρw_2^k for the O–H_2 distance) and a bond angles ρw_3^k. So, one water molecule has a total of nine degrees of freedom.

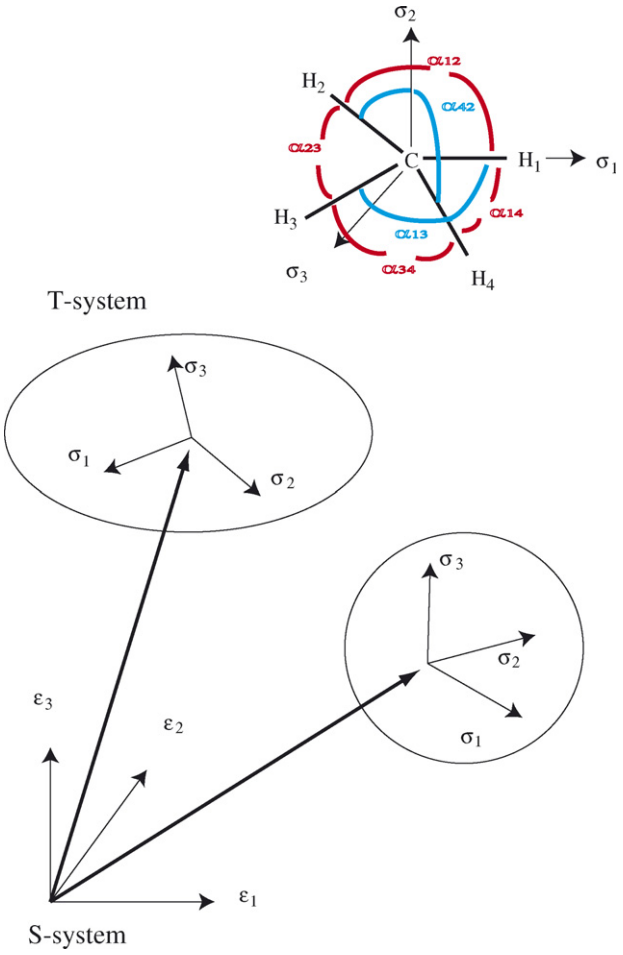

Fig. 1. The S-system is a fixed laboratory coordinate system. The T-system is on a methane. Inset: the carbon atom in a methane is placed at the origin of the T-system, and H_1 atom is on the positive x-axis, and H_2 atom lies on the plane spanned by σ_1 and σ_2. H_3 and H_4 atoms are determined by considering tetradedral angle 109.471°.

As shown in the inset of Fig. 1, the internal variables in the nth methane are specified by four bond lengths (ρ_1^n for the C–H_1, ρ_2^n for the C–H_2, ρ_3^n for the C–H_3 and ρ_4^n for the C–H_4) and six bond angles (ρ_5^n or α_{12} for H_1–C–H_2 angle, ρ_6^n or α_{13} for H_1–C–H_3, ρ_7^n or α_{14} for H_1–C–H_4, ρ_8^n or α_{34} for H_3–C–H_4, ρ_9^n or α_{24} for H_2–C–H_4 and ρ_{10}^n or α_{23} for H_2–C–H_3). So, one methane could have a total of 16 degrees of freedom, but a relationship between the six bond angles exists. Hence the real number of the degrees of freedom of a methane is 15. However, for normal mode analysis, we will introduce the necessary expressions with the 16 variables for a methane.

2.2. Modelling of methane hydrate

From the unit cell of structure I, pick a small cage and a large cage in contact with each other. The small cage is comprised of 20 water molecules, while the large cage consists of 24 water molecules. Because the cages are connected, a pentagon is shared by both. The number of water molecules in both cages together totals 39. The independent variables for the water molecules sum to 351 (=39 × 9). Each cage holds one methane. The number of independent variables for the two methanes sums to 32 (=2 × 16), and so the total number of variables is 383.

2.3. Total potential energy E of methane hydrate

The total potential energy E for methane hydrate is described as a sum of five energies as follows:

$$E = E_{\mathrm{wat}} + E_{\mathrm{wat-wat}} + E_{\mathrm{met}} + E_{\mathrm{met-met}} + E_{\mathrm{met-wat}} \tag{1}$$

The first energy E_{wat} is an intramolecular interaction of water, and expressed as:

$$E_{\mathrm{wat}} = \frac{1}{2} \sum_{\mathrm{waters}} \sum_{\nu,\mu=1}^{3} K_{\nu\mu} (\rho w_\nu^k - \rho w_{\nu,0})(\rho w_\mu^k - \rho w_{\mu,0}) \tag{2}$$

where $K_{\nu\mu}$ is a force constant for variables ρw_ν^k and ρw_μ^k; it is assumed to be the same for all water molecules. The $\rho w_{\nu,0}$ (ν = 1, 2, or 3) is the equilibrium value for each variable ρw_ν^k. These parameters were used in our previous papers and are again given in Table 1.

The second energy $E_{\mathrm{wat-wat}}$ is an intermolecular interaction between waters:

$$E_{\mathrm{wat-wat}} = \sum_{\mathrm{pairs}} \frac{1}{4\pi\varepsilon_0} \frac{q_i q_j}{r_{ij}} + \sum_{\mathrm{pairs}} \left\{ \varepsilon \left(\frac{r_0}{r_{ij}} \right)^{12} - 2\varepsilon \left(\frac{r_0}{r_{ij}} \right)^{6} \right\} + \sum_{\text{H-bonds}} \left\{ \varepsilon \left(\frac{r_0}{r_{\mathrm{HX}}} \right)^{12} - 2\varepsilon \left(\frac{r_0}{r_{\mathrm{HX}}} \right)^{10} \right\} \tag{3}$$

where the first term is an electrostatic energy. The partial charge of a water oxygen (OW) and hydrogen (HW) are −0.33 and 0.165, respectively, in units of electronic charge. ε_0 is the dielectric constant *in vacuo*. The second term is the Lennard–Jones nonbonded interaction energy of an atom pair i, j. These energy parameters were also used in the previous papers and are again shown in Table 2. The third term is a

Table 1
Intra-water potential parameters

ν	$K_{\nu 1}$	$K_{\nu 2}$	$K_{\nu 3}$	$\rho w_{\nu,0}$
1	7.61876 aJ/Å^2	−0.05288 aJ/Å^2	0.03479 aJ/(Å rad)	1.0 Å
2	−0.05288	7.61876	0.03479	1.0 Å
3	0.03479	0.03479	0.69439 aJ/rad^2	109.5°

Table 2
Nonbonded potential parameters $U_{NB} = \varepsilon(r_0/r_{ij})^{12} - 2\varepsilon(r_0/r_{ij})^6$

Atom pairs (i, j)	ε[a] (aJ)	r_0[b] (Å)
OW–OW	0.6533×10^{-3}	3.2400
HW–HW, HM–HW, HM–HM	0.3079×10^{-3}	2.8300
CM–CM	0.2636×10^{-3}	4.1200
CM–HM, CM–HW	0.2484×10^{-3}	3.4750
CM–OW	0.3905×10^{-3}	3.6800

[a] ε is the depth of the energy minimum.
[b] r_0 is the corresponding internuclear distance.

hydrogen bond potential between donor (H) and acceptor (X) atoms. The energy parameters are also shown in Table 3.

The third energy E_{met} is an intramolecular interaction of methane, and expressed as below:

$$E_{met} = \sum_{methanes} \{V^{(2)} + V^{(3)}\} \tag{4}$$

where $V^{(2)}$ describes a harmonic potential energy and $V^{(3)}$ is the cubic anharmonic potential energy, and their explicit expressions are given in Appendix A.1 [10]. First, we have to determine a set of internal coordinate force constants for harmonic potential energy. In Appendix A.2, we describe how they are determined from experimental data of methane shown in Table A1 [11].

The fourth energy $E_{met-met}$ is an intermolecular interaction between methanes, expressed as below:

$$E_{met-met} = \sum_{pairs} \frac{1}{4\pi\varepsilon} \frac{q_i q_j}{r_{ij}} + \sum_{pairs} \left\{ \varepsilon \left(\frac{r_0}{r_{ij}} \right)^{12} - 2\varepsilon \left(\frac{r_0}{r_{ij}} \right)^{6} \right\} \tag{5}$$

where the first term is an electrostatic energy. The partial charge of a methane carbon (CM) and hydrogen (HM) are set at −0.12 and 0.03, respectively, in units of electronic charge [12]. ε is $84 \times \varepsilon_0$ because water molecules exist between methanes. The second term is the nonbonded interaction energy of an atom pair i, j. The energy parameters are shown in Table 2.

Table 3
Hydrogen bond potential parameters $U_{HB} = \varepsilon(r_0/r_{HX})^{12} - 2\varepsilon(r_0/r_{HX})^{10}$

Atom pairs (H, X)	ε (aJ)	r_0 (Å)
HW–OW	$\varepsilon_W = 5.8686 \times 10^{-3}$, 4.29 ε_W[a] $= 25.1760 \times 10^{-3}$	2.2063, $0.775 r_0$[b] = 1.7099
HM–OW	$\varepsilon_M = \varepsilon_W \times 0.75$, 4.29 $\varepsilon_M = 18.8820 \times 10^{-3}$	2.2063, $0.775 r_0$ = 1.7099

[a] The depth of the energy minimum is 4.29ε.
[b] The corresponding internuclear distance is $0.775 r_0$.

The fifth energy $E_{met-wat}$ is an intermolecular interaction between methane and water:

$$E_{met-wat} = \sum_{pairs} \frac{1}{4\pi\varepsilon_0} \frac{q_i q_j}{r_{ij}} + \sum_{pairs} \left\{ \varepsilon \left(\frac{r_0}{r_{ij}} \right)^{12} - 2\varepsilon \left(\frac{r_0}{r_{ij}} \right)^{6} \right\} + \sum_{H\text{-bonds}} \left\{ \varepsilon \left(\frac{r_0}{r_{HX}} \right)^{12} - 2\varepsilon \left(\frac{r_0}{r_{HX}} \right)^{10} \right\} \tag{6}$$

where the energy parameters of the second and the third terms are given in Tables 2 and 3.

2.4. Hessian matrix for total potential energy E

The second derivatives $\partial^2 E/\partial q_i \partial q_j$ for the total potential energy E can be summarized with a single equation:

$$\frac{\partial^2 E}{\partial q_i \partial q_j} = (\phi_i, \psi_i) \left\{ s_{ij} \sum_{\xi \in M_i} \sum_{\eta \in M_j} (c_{\xi\eta} C^*_{ij} + d_{\xi\eta} D_{\xi\eta}) \right\} \begin{pmatrix} \phi_j \\ \psi_j \end{pmatrix} \tag{7}$$

Here q_i means the independent variables of each molecule in methane hydrate. See [13,14] for a derivation of Eq. (7).

3. Results

3.1. Energy minimization

The assembly comprised of a small and large cage is energy minimized using Newton's method based on a modified Cholesky factorization of the Hessian [15]. Energy minimization is stopped when the energy difference between the current step and the earlier step becomes less than 1.0×10^{-26} aJ. At this point in multidimensional space $\{t^k_\mu, \tau^k_\mu, \rho w^k_\nu, (\mu, \nu = 1\text{–}3, k = 1\text{–}39), t^n_\mu, \tau^n_\mu, \rho^n_\nu, (\mu = 1\text{–}3, \nu = 1\text{–}10, n = 1\text{–}2)\}$, the subset of the Hessian, whose elements are expressed in terms of t_μ and τ_μ had six positive eigenvalues for the respective waters and methanes. Likewise the subset expressed in terms of ρw^k_ν had three positive eigenvalues for the respective waters. Also the subset expressed in terms of ρ^n_ν had 10 positive eigenvalues for the respective methanes.

3.2. Normal mode analysis for methane

3.2.1. Internal motions analysed by normal vibrational modes

The force constant matrix F necessary to do normal mode analysis is the subset of the Hessian for each methane in the minimum energy configuration, whose elements are $\partial^2 E/\partial \rho^n_i \partial \rho^n_j$ (i, j = 1–10, n = 1–2). The kinetic energy matrix G is derived in Appendix A.3.2 following the work of Wilson [16,17]. In addition, Appendix A.3.3 shows that by using the symmetry coordinates, these matrices with 10×10 elements are reduced to matrices with 9×9 elements [18]. These matrices are denoted as F_s and G_s, respectively. With the force constant and the kinetic energy matrices (F_s and G_s), nine

Table 4
Normal vibrational frequency (cm^{-1}) of methane in cages (A_1: C–H symmetric stretch mode)

Cage	Raman spectra[a]	H-bond strength between methane and water: harmonic approximation with only $V^{(2)}$ (anharmonic approximation with $V^{(2)}$ and $V^{(3)}$)		
		ε_M	$\varepsilon_M \times 0.5$	No H-bonding
5^{12}	2915	2918.4 (2915.4)	2919.5 (2920.0)	2920.6 (2924.4)
$5^{12}6^2$	2905	2937.8 (2901.9)	2917.9 (2912.3)	2918.0 (2915.6)

[a] From Ref. [5].

normal vibrational frequencies for methane in hydrate are obtained by the GF method described in Appendix A.3.4.

At first we minimized the total potential energy E with only the harmonic potential $V^{(2)}$ in Eq. (4). Then we did normal mode analysis for each methane in the small and large cages, and obtained nine normal vibrational frequencies for each. In Table 4, we show only frequency ν_1 of the A_1 mode for each methane with the Raman spectra for small and large cages. In the total potential energy E for methane hydrate, as already described in Eq. (6), we include a hydrogen bond (H-bond) potential between methane hydrogen and water oxygen, but we naturally assume that this H-bond strength ε_M would be weaker than the H-bond strength ε_W between waters. We initially take this strength at 75% of the strength between waters: $\varepsilon_M = \varepsilon_W \times 0.75$, referred to as the intact H-bond strength. Although the other H-bond strengths are shown in Table 4, we will refer to these later. Table 4 shows that the Raman spectra indicate that the ν_1 frequency in the large cage shifts downward compared to the small cage; moreover, the frequencies in both cages are shifted downward compared to the frequency in gas (2916.5 cm^{-1} in Table A1). On the other hand, the frequencies calculated in the harmonic approximation are incorrectly shifted upward compared to in gas, and in addition, the frequency in the large cage shifts upward compared to the small cage. This result is contrary to the experimental Raman spectra. Thus we conclude that without an anharmonic potential, we cannot get results in reasonable agreement with experiment.

Hence, we again minimized the total potential energy E with a cubic anharmonic potential energy $V^{(3)}$, expressed in Eq. (4). By normal mode analysis, we obtained nine frequencies, and put the new ν_1 frequency in parentheses in Table 4. We see that the frequencies in both cages together are lower than the one in gas, and furthermore the frequency in the large cage shifts downward compared to the small cage, which is contrary to the results calculated with the harmonic approximation but in reasonable agreement with experiment. Therefore, hereinafter, we will analyse the results calculated with the anharmonic potential energy and use ε_M as the H-bond strength between methane and water.

In Fig. 2, we compare the nine calculated frequencies with the experimental Raman frequencies for gaseous and hydrated methane. We see that four frequencies in gas split into nine

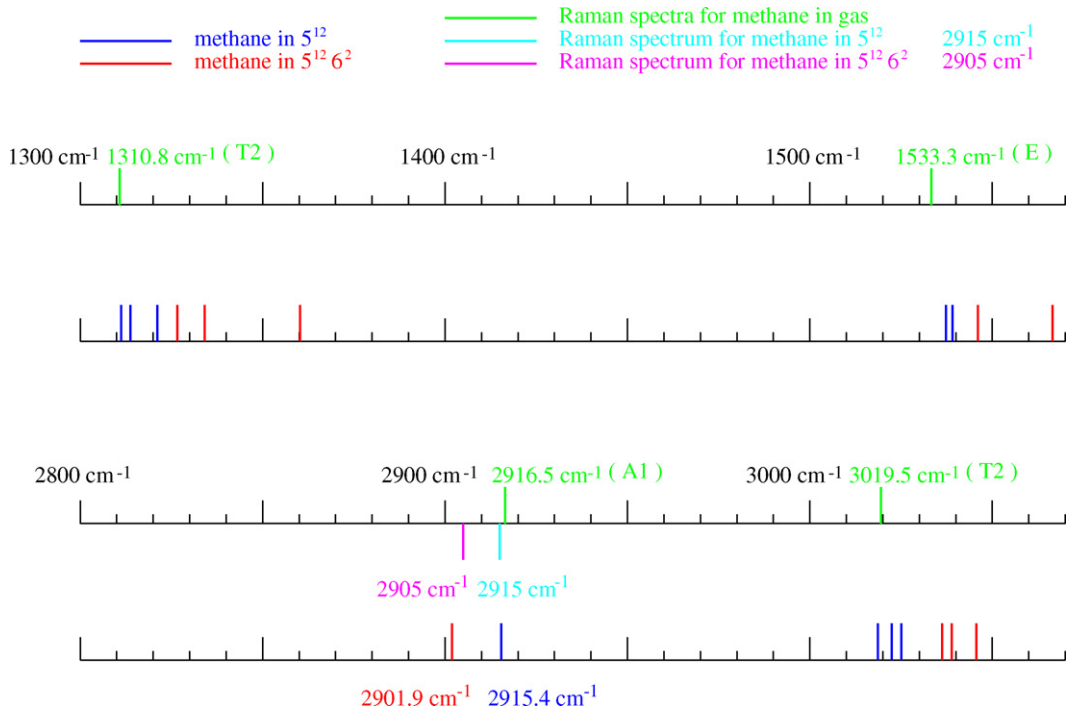

Fig. 2. Internal vibrational frequencies of methane in hydrate. The calculated frequencies are in blue for the methane in the small cage, and in red for the large. The four frequencies observed in gas are coloured in green. Raman spectra is in aqua for methane in the small cage and in magenta for the large.

frequencies due to a breakdown of the symmetry for methane in the cages: 1310.8 and 3019.5 cm^{-1} in T_2 symmetry are each separated into three lines: 1533.3 cm^{-1} in E symmetry splits into two; and 2916.5 cm^{-1} in A_1 symmetry shifts downward in both cages. In addition, as already described, we observe that the frequency in the A_1 mode in the large cage is lower than the one in the small cage, whereas, the frequencies in T_2 and E modes in the large cage are higher than the ones in the small. The reason for the last result is not yet known. We expect that future Raman and/or infrared spectra will clarify these things.

3.2.2. Atomic displacements due to internal motions

How does the normal mode excite atomic motion? To answer this question, Appendix A.4 is provided. In Fig. 3(a)–(d), we depict displacement vectors of methane atoms in the four normal vibrational modes. In these figures as well as in subsequent figures, the displacements that occur when each of the normal modes is thermally excited at 100 K are calculated. Hydrogen bonds are depicted in dashed lines. As a criterion of H-bonding between waters, we assume as before [7] that a hydrogen–acceptor distance must be less than 2.5 Å, and a donor–hydrogen–acceptor angle must be larger than 135°. On the other hand, since we assume that H-bonding between methane and water is weaker than between waters, we set as a criterion of H-bonding that an HM–OW distance must be less than 2.8 Å, and a CM–HM–OW angle must be larger than 135° as well. Using this criterion, we get three H-bonding interactions of 2.55, 2.60 and 2.64 Å in the small cage, and three of 1.84, 1.85 and 2.55 Å in the large cage.

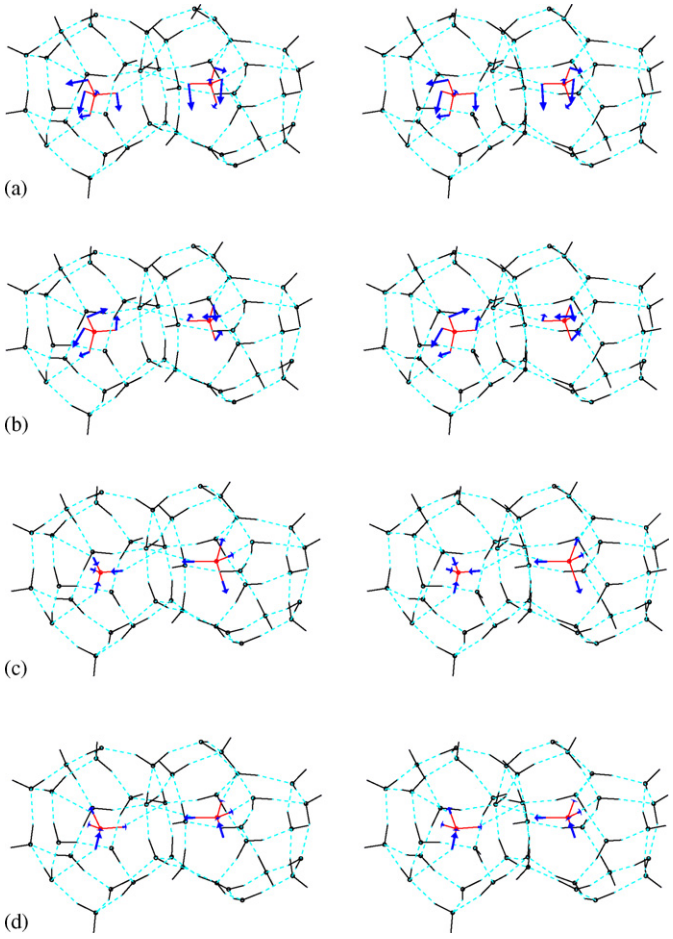

Fig. 3. Stereo view of displacement vectors of methane atoms (in red) in the small and large cages. Root-mean-square displacements (rmsDs) of atoms are shown by vectors (in blue) that are magnified 70 times for easy perception. rmsDs for carbon and hydrogen are described as (value_c, value_h) × 10^{-3} Å. (a) The lowest mode with frequencies of 1311.2 cm^{-1} (4.2, 17) as rmsDs for the small cage and 1326.7 cm^{-1} (4.0, 17) for the large cage, which is chosen from three modes of T_2 symmetry. (b) The 5th lowest mode with frequencies of 1539.1 cm^{-1} (0.13, 16) for small and 1566.5 cm^{-1} (0.43, 15) for large, chosen from two modes of E symmetry. (c) The 6th mode with frequencies of 2915.4 cm^{-1} (0.028, 8.3) for small and 2901.9 cm^{-1} (0.20, 8.3) for large, corresponding to A_1 symmetry. (d) The 7th mode with frequencies of 3018.6 cm^{-1} (1.5, 7.6) for small and 3036.3 cm^{-1} (1.5, 7.5) for large, chosen from three modes of T_2 symmetry.

3.2.3. Ellipsoid of internal motions due to thermal vibration

With the mean-square displacement matrix expressed by Eq. (A-15) including the nine normal vibrational modes, anisotropic thermal vibrations for each methane atom in the small and large cages are drawn in Fig. 4 [19].

3.2.4. A rigid-body motion analysed by normal vibrational mode

The force constant matrix F of a rigid-body motion for each methane is the subset of the Hessian obtained at the energy minimum point, having six positive eigenvalues. The kinetic energy matrix H for a rigid molecule expressed in terms of a translational vector and Eulerian angles is given in [20]. With the kinetic and force constant matrices (H and F), normal vibrational modes for each methane are obtained by solving the generalized eigenvalue equation:

$$F\Delta\boldsymbol{u} = (2\pi\nu_\alpha)^2 H\Delta\boldsymbol{u}$$

where ν_α is the frequency of the αth normal mode. The $\Delta\boldsymbol{u}$ is a six-dimensional column vector, whose elements are (Δt_1, Δt_2, Δt_3, $\Delta\tau_1$, $\Delta\tau_2$, $\Delta\tau_3$). This vector $\Delta\boldsymbol{u}$ expressing the changes of the translating vector and the Eulerian angles is converted into changes Δr in atomic coordinates of the methane atoms by a series of mathematical manipulations, which are given in [20]. Thus the mean-square displacement matrix of the atom caused by the rigid-body motion of a methane is obtained. The six vibrational frequencies of a rigid-body motion for each methane are

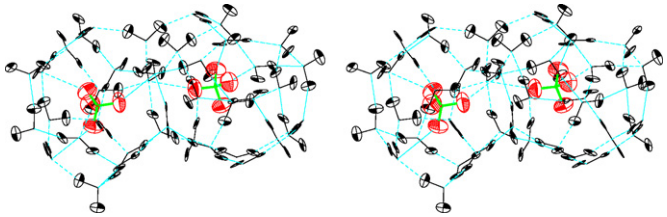

Fig. 4. Stereo view of internal motions of all the atoms in the methane hydrate model system. The thermal ellipsoids of atoms (at 100% probability) are drawn with ORTEP and are magnified 14.42^3 (=3000) times for easy perception. The ellipsoids of carbon and the bonds of methane are in green. The rmsDs for carbon and hydrogen are (7.6, 39.8) × 10^{-3} Å for the small cage and are (7.4, 39.3) × 10^{-3} Å for the large.

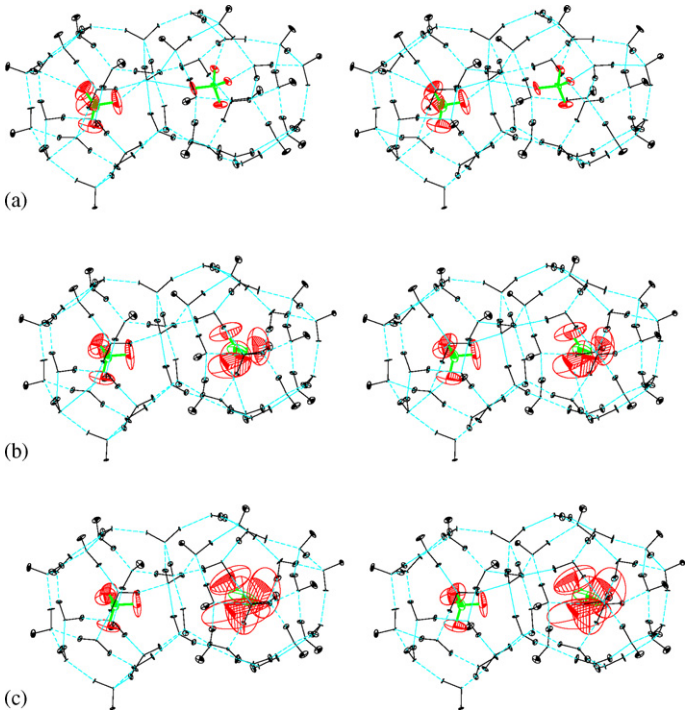

Fig. 5. Stereo view of rigid-body motions of each molecule in the methane hydrate model system. The thermal ellipsoids of atoms are drawn at 100% probability. The ellipsoids of carbon and the bonds of methane are in green. The rmsDs for carbon and hydrogen are described as (value_*c* Å, value_*h* Å). (a) Calculated with the intact H-bond strength. The rmsDs are (0.355 Å, 0.634 Å) for the small, (0.184 Å, 0.289 Å) for the large. (b) Calculated with the half H-bond strength. The rmsDs are (0.337 Å, 0.634 Å) for the small, (0.538 Å, 1.014 Å) for the large. (c) Calculated with no H-bond strength. The rmsDs are (0.297 Å, 0.579 Å) for the small, (0.697 Å, 1.416 Å) for the large.

Table 5
Six normal vibrational frequencies (cm^{-1}) for a rigid-body motion of methane in cages

Normal mode	H-bond strength between methane and water					
	ε_M		$\varepsilon_M \times 0.5$		No H-bonding	
	5^{12}	$5^{12}6^2$	5^{12}	$5^{12}6^2$	5^{12}	$5^{12}6^2$
Lowest	43.9	74.6	43.8	28.3	52.5	17.5
2nd	59.8	155.7	65.4	38.9	70.7	32.4
3rd	68.1	170.8	74.0	42.5	78.8	35.0
4th	85.4	200.5	84.5	55.8	90.2	49.6
5th	91.6	215.1	94.8	62.6	100.4	59.4
6th	127.9	258.3	110.0	70.7	111.8	71.4

shown in Table 5. Regarding the vector $\Delta\boldsymbol{u}$, we get $\Delta\boldsymbol{u}$ = (−0.282, −0.179, 0.220 Å; 16.8°, −19.2°, −18.7°) for methane in the small cage, and (0.149, 0.103, 0.080 Å; 1.68°, −10.5°, 1.89°) in the large. Then, with the mean-square displacement matrix calculated using $\Delta\boldsymbol{u}$, anisotropic thermal vibrations for all atoms in the methanes are depicted in Fig. 5(a). Reflecting the lower frequencies in the small cage in Table 5, the thermal ellipsoids in the small cage are larger than the large. This result is also reflected numerically by the rmsD.

3.3. Normal mode analysis for water molecule

Internal motions and rigid-body motions of water molecules are already described in our early papers [7,8,20]. The results for waters with methanes are shown in Figs. 4 and 5.

4. Discussion and conclusion

First, we calculated the volumes of both the small and the large cages, and we found the volume of large cage is about $\sqrt{2}$ times the small. On the other hand, our calculations for the thermal ellipsoids of methane atoms show them larger for the small cage than for the large cage. This result seems unreasonable. So, to check whether our calculations are valid, we reduced the H-bond strength between methane and water to half, and then to zero. With the new H-bond strengths, we energy minimised the total potential energy E in the two cases of with and without an anharmonic potential, and then we did the normal mode analyses for internal motions of methane and for rigid-body motions. In Table 5, we show the six normal vibrational frequencies for a rigid-body motion only for the structures minimised with the anharmonic potential. We see that the vibrational frequencies in the large cage shift more downward as the H-bond strength is decreased, whereas, the shift in frequencies in the small cage do not clearly depend on H-bond strength. At half strength, the frequency of the 6th mode apparently reduces in comparison with the intact strength, but the frequencies of the 2nd, 3rd and 5th modes increase, and the frequencies in the lowest and 4th modes reduce slightly. When the H-bond strength changes from half to zero, all the frequencies in the small cage increase, and comparing the intact strength and zero, all the frequencies except for the 6th mode increase. These results for the small cage seem to arise from a subtle

relationship between the size of cage and the existence of H-bonding.

With the frequencies shown in Table 5, we figure the thermal ellipsoids in Fig. 5(b)–(c). We see in Fig. 5(b) that, consistent with the lower frequencies in the large cage, the thermal ellipsoids in the large cage are larger than the small cage. This finding seems to be reasonable since the large cage has a volume of $\sqrt{2}$ times the small. When we look at Fig. 5(c), figured with no H-bonding, the thermal ellipsoids in the large cage are much larger than the ones figured at half strength, whereas, the ones in the small cage are tiny compared to ones figured at half strength, which is numerically indicated by rmsDs of carbon and hydrogen.

Let us again compare the thermal ellipsoids of methanes in Fig. 5(a), estimated with the intact H-bond strength, and those in Fig. 5(b), with the half H-bond strength. In regard to the sizes of ellipsoids in the small cages, the figures are similar, which is also numerically indicated by rmsDs of carbon and hydrogen. In regard to the sizes of ellipsoids in the large cage, those in Fig. 5(b) are larger than those in Fig. 5(a). The methane in Fig. 5(b) is almost in the middle of the large cage, whereas, the methane in Fig. 5(a) is offset from the middle toward the pentagon shared with the cages. This displacement may arise from H-bonding interactions. In Fig. 5(a), calculated with the intact H-bond strength, as we have already described, there are three H-bonding interactions of 1.84, 1.85 and 2.55 Å (HM–OW distance) in the large cage. On the other hand, as we can see in Fig. 5(b), calculated at half strength, there is only one H-bonding interaction at 2.76 Å.

Thus from a point of H-bond strength, the methane of Fig. 5(b), evaluated at half strength, seems to be acceptable. Why do we not apply this H-bond strength between methane and water? To answer this question, Table 4 is provided. In this table, the normal vibrational frequency ν_1 of mode A_1, calculated both with and without the anharmonic potential, in the three cases of the intact H-bond strength, half strength and no H-bonding are shown. If we calculate the normal frequency ν_1 with the anharmonic potential, regardless of whether the H-bond strength exists, we get a result that the ν_1 frequency in the large cage is shifted downward compared to the ν_1 frequency in the small cage, which is in agreement with the relative experimental frequencies. But the Raman spectra ν_1 observed in both hydrate cages are lower than the frequency observed in gaseous methane (2916.5 cm^{-1}). In this regard, the ν_1 frequencies calculated only with the intact H-bond strength are in agreement with the Raman spectra. Hence, we abandon our analyses with the half H-bond strength and no H-bonding, even though the sizes of the thermal ellipsoids seem to be reasonable.

How do we produce the probable thermal ellipsoids of methane in the large cage, with the intact H-bond strength? Methane hydrate observed by Raman spectroscopy consists of numerous small and large cages piled against each other. Therefore, two cages as modeled here are not sufficient. To get an acceptable result, it is apparently necessary to position a large cage, which is $5^{12}6^2$ at a centre and to enclose the cage by at least 14 polyhedra of small and large cages. Thus we could make a larger model system of methane hydrate focussed on the large cage. We are now planning such a study.

Table 6
A relationship between a change of bond length and H-bond strength between methane and water

	ε_M		$\varepsilon_M \times 0.5$	
	HM–OW distance (Å)	$\Delta\rho_{i,mod}$ (%)	HM–OW distance (Å)	$\Delta\rho_{i,mod}$ (%)
5^{12}	2.55	0.02	2.71	0.02
	2.60	−0.01	2.79	0.00
	2.64	0.04		
$5^{12}6^2$	1.84	0.45	2.76	0.02
	1.85	0.43		
	2.55	0.02		

Modulus of bond length: $\Delta\rho_{i,mod} = (\rho_i - \rho_{i,0})/\rho_{i,0} \times 100$ $(i = 1–4)$ $\rho_{i,0}$ = 1.0858 Å.

We observe a relationship between a change in the bond length of methane hydrogen (HM) participating as donor in H-bonding to water oxygen (OW) and the H-bond strength. In Table 6, we show the distance from a donor HM to an acceptor OW, as well as the ratio of the change in bond length of HM to the equilibrium bond length: $\Delta\rho_{i,mod} = (\rho_i - \rho_{i,0})/\rho_{i,0} \times 100$. We see the three H-bonding interactions in both cages in the case of the intact H-bond strength, and three in the case of half strength. In these nine H-bonding interactions, we realize that as the HM-OW distance gets shorter, the H-bond would strengthen, and then the modulus of bond length is generally getting larger, that is, the C–H bond length gets longer. This increase in bond length causes changes of the anharmonic potential energy $V^{(3)}$ as expressed in Eq. (A-2), and then it affects the normal vibrational frequencies, as shown in Table 4. The tabulated data clearly exhibit that two strong H-bondings of 1.84 and 1.85 Å in the large cage have an effect on the anharmonic potential energy: the ν_1 frequency calculated with the anharmonic potential is shifted downward in comparison to the frequency calculated with the harmonic approximation. Thus there is a close relationship between the dynamical structure of methane and the H-bond strength between methane and water.

Very recently, a paper describing a molecular dynamics simulation of methane hydrate was published, in which Greathouse et al. suggest that it might be worth considering that the experimental peak at 2915 cm^{-1} is due to methane molecules in large cages, not small cages [21]. This suggestion is contrary to the interpretation of Sloan Jr. and co-workers to intensity peaks produced via Raman spectroscopy [5] and also contrary to our standpoint based on that Raman data. Tse's work using a density functional dynamics method [22] appears to support the interpretation of Sloan Jr. and co-workers. In addition, other work using molecular dynamics simulations [23] seems to support the viewpoint of Sloan Jr. and co-workers. To clear up this controversy, we perform two calculations.

The first calculation is as follows: in Table 4, we already show the ν_1 frequency of methanes in both cages for three H-bond strengths between methane and water, in the two cases of with and without the anharmonic potential. In addition to these calculations, we further calculated the ν_1 frequency in both

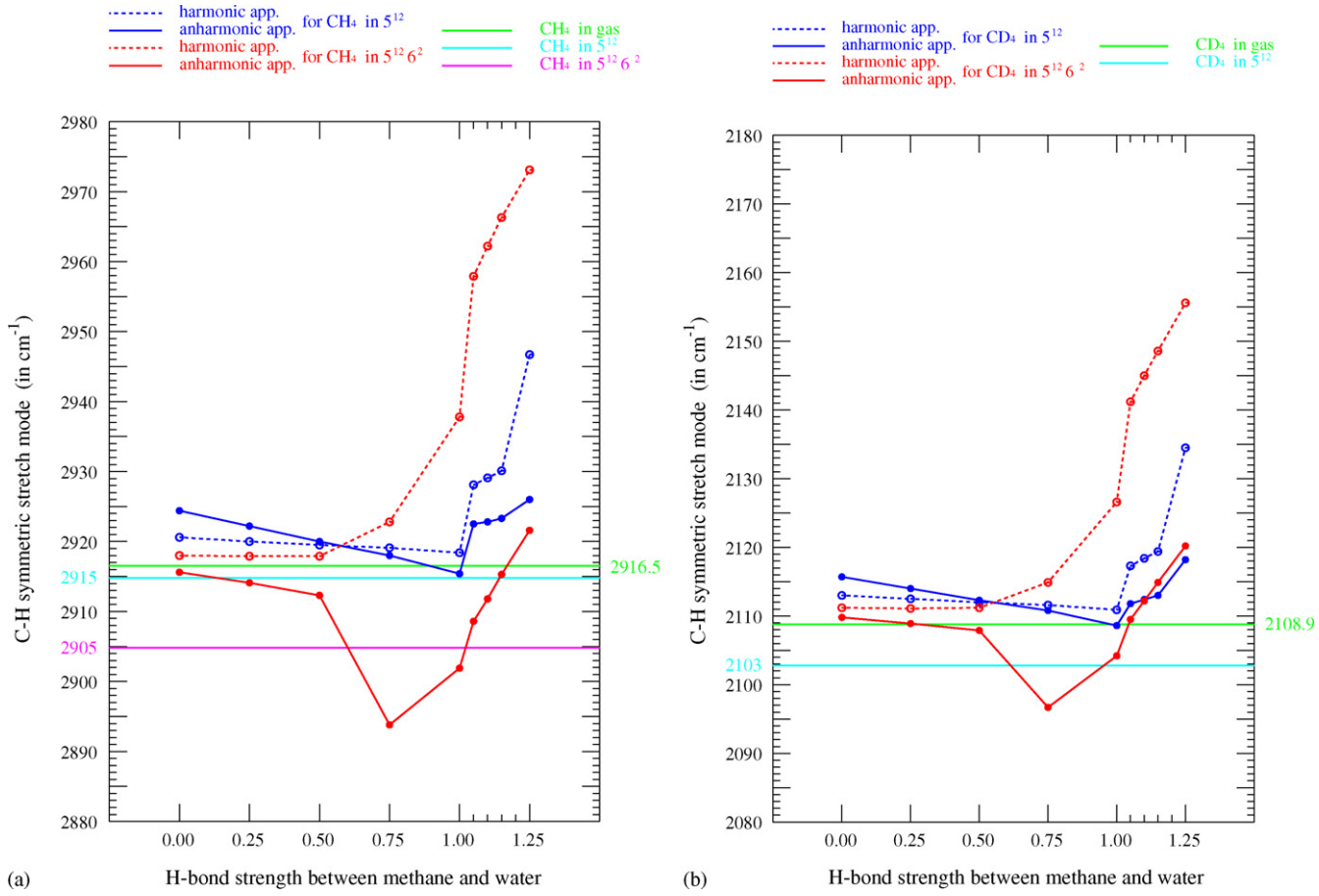

Fig. 6. C–H symmetric stretch mode ν_1 (in units of cm^{-1}) vs. H-bond strength between methane and water (in units of ε_M). The dashed lines correspond to the harmonic approximation with only $V^{(2)}$, whereas, the solid lines correspond to the anharmonic approximation with $V^{(2)}$ and $V^{(3)}$. The blue indicates the quantities of the small cage, whereas, the red indicates the large cage. The green line shows the frequency in gaseous methane, the aqua shows the one in the small cage speculated by Raman scattering, and the magenta shows the one in the large. (a) For CH_4 (b) For CD_4.

cages for a wide range of H-bond strengths. This result is depicted in Fig. 6(a). This figure definitely shows we cannot obtain a frequency lower than 2916.5 cm^{-1} found in gaseous methane via the harmonic approximation in our model system composed of two cages. With the anharmonic approximation, we can get a result that 2905 cm^{-1} is probably a frequency in the large cage, whereas, 2915 cm^{-1} could be a frequency in either the small or large. Because of the energy parameters adopted in our model system, the H-bond strength between methane and water should be the same for both cages. Therefore, one of frequencies, calculated with values of the H-bond strength near the intact strength ε_M, belongs to the small cage and the other frequency belongs to the large. We believe that 2915 cm^{-1} is probably a frequency in the small cage. Hence our calculated results appear to support the speculation of Sloan Jr. and co-workers.

Sloan Jr. and co-workers also did Raman experiments of deuterated methane (CD_4) + propane (C_3H_8) in structure II hydrate [5]. The authors observed that the Raman spectrum for CD_4 shows a very broad band with a small shoulder and a long tail at the low wavenumber side. The major band centered at 2103 cm^{-1} corresponds to CD_4 in the small cavity of sII, and the shoulder contributing to the long tail is for CD_4 in the large cavity of sII. Because C_3H_8 only occupies the large cavity, one expects to find a very small amount of CD_4 in the large cavity. We did calculations to see whether we could produce the Raman spectra of Sloan Jr. and co-workers for sII.

The second calculation is as follows. First, it is necessary to choose a harmonic internal coordinate force constant for CD_4. We did this via the experimental data of CD_4 shown in Table A1. The values obtained are put in parentheses in Table A2. Likewise, as we did for CH_4, we energy minimised and did normal mode analysis. We show our calculation's results in Fig. 6(b). As in the case of CH_4, we cannot obtain a frequency lower than 2108.9 cm^{-1} in gaseous CD_4 with the harmonic approximation. On the other hand, with an anharmonic approximation, we see that frequencies in the small cage are shifted a bit lower than 2108.9 cm^{-1} only in a very narrow range of H-bond strengths, whereas, frequencies in the large cage are shifted below 2108.9 cm^{-1} through a wide range of possible H-bond strengths. By assuming the potential energy parameters, except for the harmonic force constants, are not dependent on mass, we did calculations for CD_4. Thus as likely in the case of CH_4, our calculations for CD_4 seem to support the explanation of Sloan Jr. and co-workers.

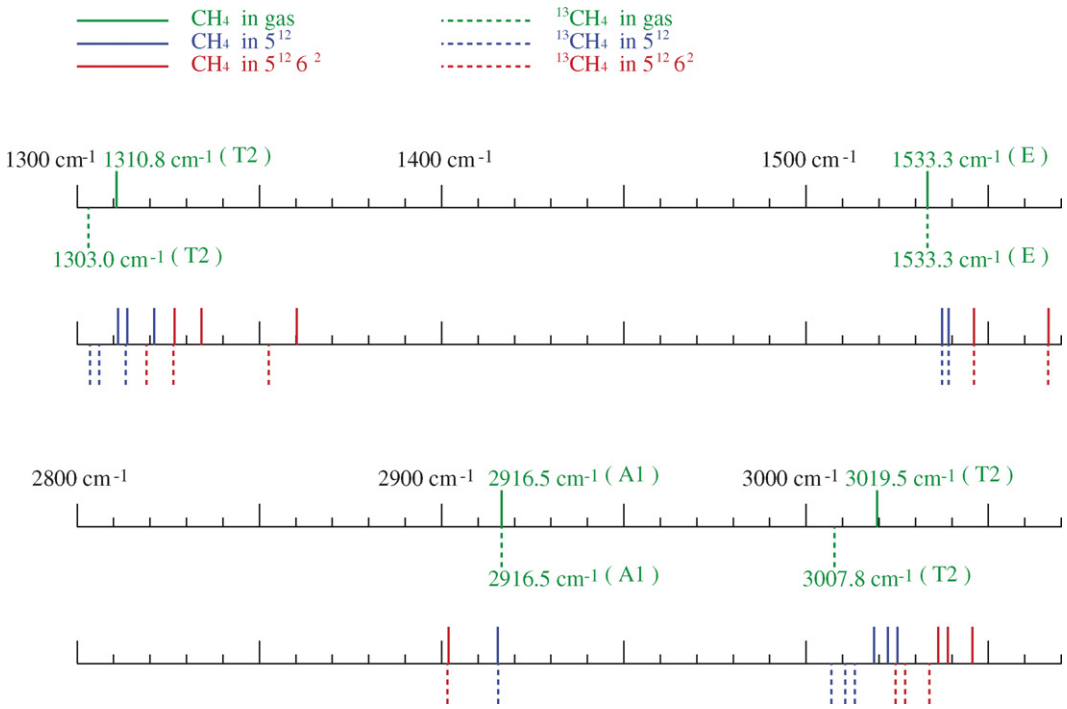

Fig. 7. Internal vibrational frequencies of $^{13}CH_4$ in hydrate. The solid lines exhibit frequencies in CH_4, whereas, the dashed lines for $^{13}CH_4$. The calculated frequencies are in blue for the methane in the small cage, and in red for the large. The four frequencies observed in gaseous CH_4 are coloured in green with a solid line, whereas, the four frequencies calculated in gaseous $^{13}CH_4$ are in green with a dashed line.

Let us compare the root-mean-square displacement of CD_4 to that of CH_4. The values are calculated at the intact H-bond strength with the anharmonic potential. The rmsDs for carbon and deuterium, respectively, are $(11.9, 37.1) \times 10^{-3}$ Å for the small cage and are $(11.7, 36.6) \times 10^{-3}$ Å for the large. Comparing with those of CH_4 (see Fig. 4), rmsD of deuterium is a bit compressed compared to hydrogen, due to having the twice mass of the hydrogen, while on the contrary the carbon in CD_4 bonded by heavy hydrogens is more mobile than in CH_4 bonded by light hydrogens, although the movement is very tiny.

Additionally, we did calculations on the heavy carbon isotopomer $^{13}CH_4$ because our calculations could predict a useful information on frequencies for experimentalists. Except for the mass of carbon, we assume the energy parameters in $^{13}CH_4$ are the same as in CH_4. Fig. 7 is provided to visualize clearly the differences between $^{13}CH_4$ and CH_4. We see that the ν_1 frequency (A_1 mode) and ν_2 frequency (E mode) are the same in CH_4 and $^{13}CH_4$ in gaseous phase, since the A_1 mode is bond stretching mode and E mode is angle bending mode, and both modes are gerade. Both modes give the same frequencies in CH_4 and $^{13}CH_4$ in the hydrated phase, although separated in the small and large cages. On the other hand, in the two T_2 modes, which are mixed modes of bond stretching and angle bending, frequencies in $^{13}CH_4$ are lower than in CH_4 in gaseous and hydrated phases due to the more massive carbon.

In conclusion, from analyses done so far, we concur with the speculation of Sloan Jr. and co-workers regarding Raman scattering. We find that when studying internal motions and rigid-body motions of methane in hydrate, it is necessary to include at least a cubic anharmonic potential energy within methane. And it is essential to consider H-bonding interactions between methane and waters: The H-bonding strength that works best is near to the intact strength ε_M. With the independent molecule model, we can generally explain Raman spectra observed in methane hydrate. Furthermore, we can estimate the atomic displacements caused by thermal vibrations, and we can express the movements of methane in the hydrate. Thus, the independent molecule model is useful for delineating the dynamical structure of each molecule in a condensed phase molecular system.

Appendix A

A.1. Harmonic and anharmonic potential energy

The internal coordinates used here are the increase $\Delta\rho_i$ ($=\rho_i - \rho_{i,0}$, $i = 1$–4) in the length of the ith bond from its equilibrium value $\rho_{i,0}$ and the increase $\Delta\alpha_{ij}$ ($=\alpha_{ij} - \alpha_{ij,0}$, $i = 1$–3, $j = 2$–4, $i < j$) in the angle between ith and jth bonds with respect to the equilibrium tetrahedral angle $\alpha_{ij,0}$. The equilibrium values are given in Table A1.

Following the notation of Raynes et al. [10], we use subscript r, s, t to denote bond stretching and α, β, γ, …, ω to denote angle bending. Thus f_{rrs} is a cubic internal coordinate force constant of the stretch–stretch–stretch type which multiplies the combination $\Delta\rho_1^2\Delta\rho_2 + \Delta\rho_1^2\Delta\rho_3 + \cdots$, whereas, f_{rst} is one which multiplies $\Delta\rho_1\Delta\rho_2\Delta\rho_3 + \Delta\rho_1\Delta\rho_2\Delta\rho_4 \ldots$. For angle bending the situation is a little more complicated because for any given angle a second angle may be adjacent or opposite. Generally, a subscript α denotes the angle first defined, an angle adjacent to a particular bond or the angle lying between two bonds. β, γ and δ are used for angles adjacent to α, and ω is used

Table A1
Parameters used for methane

Equilibrium bond length $\rho_{i,0} = 1.0858$ Å ($i = 1$–4)[a]
Equilibrium tetradedral angle, $\alpha_{ij,0} = 109.471^\circ$ ($i = 1$–3, $j = 2$–4, $i < j$)
Mass of carbon $m_C = 12$ u
Mass of hydrogen $m_H = 1.00727$ u
Mass of deuterium $m_D = 2.0140$ u

	CH_4	CD_4
Normal vibrational frequency (in units of cm^{-1})		
ν_1 (A_1)	2916.5	2108.9
ν_2 (E)	1533.3	1091.7
ν_3 (T_2)	3019.5	2260.1
ν_4 (T_2)	1310.8	997.9

[a] From Ref. [24].

for the angle opposite α. Thus $f_{r\alpha\omega}$ is of the stretch–bend–bend type and multiplies $\Delta\rho_1\Delta\alpha_{12}\Delta\alpha_{34} + \Delta\rho_1\Delta\alpha_{13}\Delta\alpha_{24} + \cdots$.

Using internal coordinates, one can express a harmonic potential energy $V^{(2)}$ for methane by:

$$\begin{aligned}2V^{(2)} = {} & f_{rr}(\Delta\rho_1^2;4) + 2f_{rs}(\Delta\rho_1\Delta\rho_2;6) \\ & + f_{\alpha\alpha}(\Delta\alpha_{12}^2;6) + 2f_{\alpha\beta}(\Delta\alpha_{12}\Delta\alpha_{13};12) \\ & + 2f_{\alpha\omega}(\Delta\alpha_{12}\Delta\alpha_{34};3) + 2f_{r\beta}(\Delta\rho_1\Delta\alpha_{23};12) \\ & + 2f_{r\alpha}(\Delta\rho_1\Delta\alpha_{12};12),\end{aligned} \tag{A-1}$$

in which, following Raynes et al., we have used an abbreviated form where the parentheses contain a typical product of internal coordinates together with the total number of products of that type. The values of the harmonic internal coordinate force constant determined by the method described in the following Appendix A.2 are given in Table A2.

As for a cubic anharmonic potential energy $V^{(3)}$, we have:

$$\begin{aligned}6V^{(3)} = {} & f_{rrr}(\Delta\rho_1^3;4) + 3f_{rrs}(\Delta\rho_1^2\Delta\rho_2;12) \\ & + 6f_{rst}(\Delta\rho_1\Delta\rho_2\Delta\rho_3;4) + 3f_{rr\alpha}(\Delta\rho_1^2\Delta\alpha_{12};12) \\ & + 3f_{rr\beta}(\Delta\rho_1^2\Delta\alpha_{23};12) + 6f_{rs\alpha}(\Delta\rho_1\Delta\rho_2\Delta\alpha_{12};6) \\ & + 6f_{rs\beta}(\Delta\rho_1\Delta\rho_2\Delta\alpha_{13};24) + 6f_{rs\omega}(\Delta\rho_1\Delta\rho_2\Delta\alpha_{34};6) \\ & + 3f_{r\alpha\alpha}(\Delta\rho_1\Delta\alpha_{12}^2;12) + 3f_{r\beta\beta}(\Delta\rho_1\Delta\alpha_{23}^2;12) \\ & + 6f_{r\alpha\beta}(\Delta\rho_1\Delta\alpha_{12}\Delta\alpha_{13};12) \\ & + 6f_{r\alpha\gamma}(\Delta\rho_1\Delta\alpha_{12}\Delta\alpha_{23};24) \\ & + 6f_{r\gamma\delta}(\Delta\rho_1\Delta\alpha_{23}\Delta\alpha_{24};12) \\ & + 6f_{r\alpha\omega}(\Delta\rho_1\Delta\alpha_{12}\Delta\alpha_{34};12) \\ & + f_{\alpha\alpha\alpha}(\Delta\alpha_{12}^3;6) + 3f_{\alpha\alpha\beta}(\Delta\alpha_{12}^2\Delta\alpha_{13};24) \\ & + 3f_{\alpha\alpha\omega}(\Delta\alpha_{12}^2\Delta\alpha_{34};6) + 6f_{\alpha\beta\gamma}(\Delta\alpha_{12}\Delta\alpha_{13}\Delta\alpha_{14};4) \\ & + 6f_{\alpha\beta\delta}(\Delta\alpha_{12}\Delta\alpha_{13}\Delta\alpha_{23};4) \\ & + 6f_{\alpha\beta\omega}(\Delta\alpha_{12}\Delta\alpha_{13}\Delta\alpha_{34};12),\end{aligned} \tag{A-2}$$

where the values of the anharmonic internal coordinate force constant are given in Table A3 and are a result of Gray and Robiette [24].

Table A2
Harmonic internal coordinate force constant of CH_4 (CD_4)

aJ/Å^2	aJ/(Å rad)	aJ/rad^2
f_{rr}: 4.92462 (5.03187)	$f_{r\alpha}$: 0.13152 (0.11314)	$f_{\alpha\alpha}$: 0.50833 (0.51938)
f_{rs}: 0.04113 (0.08354)	$f_{r\beta}$: 0.06576 (0.05657)	$f_{\alpha\beta}$: −0.01600 (−0.01457)
		$f_{\alpha\omega}$: 0.00800 (0.00729)

A.2. Determination of force constant of harmonic potential

First, we show the relationship between the symmetry coordinates and the internal coordinates:

$$\begin{aligned}S_1 &= \frac{1}{2}(\Delta\rho_1 + \Delta\rho_2 + \Delta\rho_3 + \Delta\rho_4), \\ S_{2a} &= \frac{1}{\sqrt{12}}(2\Delta\alpha_{12} - \Delta\alpha_{13} - \Delta\alpha_{14} - \Delta\alpha_{23} - \Delta\alpha_{24} + 2\Delta\alpha_{34}), \\ S_{2b} &= \frac{1}{2}(\Delta\alpha_{13} - \Delta\alpha_{14} - \Delta\alpha_{23} + \Delta\alpha_{24}), \\ S_{3x} &= \frac{1}{2}(\Delta\rho_1 - \Delta\rho_2 + \Delta\rho_3 - \Delta\rho_4), \\ S_{3y} &= \frac{1}{2}(\Delta\rho_1 - \Delta\rho_2 - \Delta\rho_3 + \Delta\rho_4), \\ S_{3z} &= \frac{1}{2}(\Delta\rho_1 + \Delta\rho_2 - \Delta\rho_3 - \Delta\rho_4), \quad S_{4x} = \frac{1}{\sqrt{2}}(\Delta\alpha_{24} - \Delta\alpha_{13}), \\ S_{4y} &= \frac{1}{\sqrt{2}}(\Delta\alpha_{23} - \Delta\alpha_{14}), \quad S_{4z} = \frac{1}{\sqrt{2}}(\Delta\alpha_{34} - \Delta\alpha_{12}).\end{aligned} \tag{A-3}$$

If a methane exists *in vacuo*, a methane has four internal vibrational modes given in Table A1. Then the harmonic potential energy $V^{(2)}$ is expressed in terms of symmetry coordinates, as done by Raynes et al.:

$$\begin{aligned}2V^{(2)} = {} & F_{11}S_1^2 + F_{22}(S_{2a}^2 + S_{2b}^2) + F_{33}(S_{3x}^2 + S_{3y}^2 + S_{3z}^2) \\ & + 2F_{34}(S_{3x}S_{4x} + S_{3y}S_{4y} + S_{3z}S_{4z}) \\ & + F_{44}(S_{4x}^2 + S_{4y}^2 + S_{4z}^2),\end{aligned} \tag{A-4}$$

Table A3
Anharmonic internal coordinate force constant

aJ/Å^3	aJ/(Å^2 rad)
f_{rrr}: −17.60250	$f_{rr\alpha}$: 0.07142
f_{rrs}: 0.09375	$f_{rr\beta}$: −0.07142
f_{rst}: −5.88000	$f_{rs\alpha}$: −0.22490
	$f_{rs\beta}$: −0.05341
	$f_{rs\omega}$: 0.01128
aJ/(Å rad^2)	aJ/rad^3
$f_{r\alpha\alpha}$: −0.14265	$f_{\alpha\alpha\alpha}$: −0.25124
$f_{r\beta\beta}$: −0.01201	$f_{\alpha\alpha\beta}$: 0.03584
$f_{r\alpha\beta}$: 0.03233	$f_{\alpha\alpha\omega}$: 0.10787
$f_{r\alpha\gamma}$: 0.05017	$f_{\alpha\beta\gamma}$: −0.10389
$f_{r\gamma\delta}$: −0.03299	$f_{\alpha\beta\delta}$: 0.14007
$f_{r\alpha\omega}$: −0.02233	$f_{\alpha\beta\omega}$: −0.05393

where F_{11}, etc., are the symmetry coordinate force constants. Using Eq. (A-3), we get the following:

$$\begin{aligned}2V^{(2)} &= F_{11}\frac{1}{4}(A+2B)+F_{22}\frac{1}{3}(C-D+2E)\\ &+F_{33}\frac{1}{4}(3A-2B)+2F_{34}\frac{1}{2\sqrt{2}}(H-I)\\ &+F_{44}\frac{1}{2}(C-2E)=A\left(\frac{1}{4}F_{11}+\frac{3}{4}F_{33}\right)\\ &+B\left(\frac{1}{2}F_{11}-\frac{1}{2}F_{33}\right)+C\left(\frac{1}{3}F_{22}+\frac{1}{2}F_{44}\right)\\ &+D\left(-\frac{1}{3}F_{22}\right)+E\left(\frac{2}{3}F_{22}-F_{44}\right)+H\left(\frac{1}{\sqrt{2}}F_{34}\right)\\ &+I\left(-\frac{1}{\sqrt{2}}F_{34}\right)=Af_{rr}+2Bf_{rs}+Cf_{\alpha\alpha}+2Df_{\alpha\beta}\\ &+2Ef_{\alpha\upsilon}+2Hf_{r\beta}+2If_{r\alpha}\end{aligned}\tag{A-5}$$

where

$$\begin{aligned}A &= \Delta\rho_1\Delta\rho_1+\Delta\rho_2\Delta\rho_2+\Delta\rho_3\Delta\rho_3+\Delta\rho_4\Delta\rho_4,\\ B &= (\Delta\rho_1\Delta\rho_3+\Delta\rho_2\Delta\rho_4)+(\Delta\rho_1\Delta\rho_4+\Delta\rho_2\Delta\rho_3)\\ &\quad+(\Delta\rho_1\Delta\rho_2+\Delta\rho_3\Delta\rho_4)=B_x+B_y+B_z\,(\text{values in each}\\ &\quad\text{parentheses correspond to each respective } B_i),\\ C &= (\Delta\alpha_{13}\Delta\alpha_{13}+\Delta\alpha_{24}\Delta\alpha_{24})+(\Delta\alpha_{14}\Delta\alpha_{14}+\Delta\alpha_{23}\Delta\alpha_{23})\\ &\quad+(\Delta\alpha_{12}\Delta\alpha_{12}+\Delta\alpha_{34}\Delta\alpha_{34})=C_x+C_y+C_z,\\ D_a &= \Delta\alpha_{13}\Delta\alpha_{14}+\Delta\alpha_{13}\Delta\alpha_{23}+\Delta\alpha_{14}\Delta\alpha_{24}+\Delta\alpha_{23}\Delta\alpha_{24},\\ D &= D_a+\Delta\alpha_{12}\Delta\alpha_{13}+\Delta\alpha_{12}\Delta\alpha_{14}+\Delta\alpha_{12}\Delta\alpha_{23}+\Delta\alpha_{12}\Delta\alpha_{24}\\ &\quad+\Delta\alpha_{13}\Delta\alpha_{34}+\Delta\alpha_{14}\Delta\alpha_{34}+\Delta\alpha_{23}\Delta\alpha_{34}+\Delta\alpha_{24}\Delta\alpha_{34},\\ E &= (\Delta\alpha_{13}\Delta\alpha_{24})+(\Delta\alpha_{14}\Delta\alpha_{23})+(\Delta\alpha_{12}\Delta\alpha_{34})\\ &\quad=E_x+E_y+E_z,\\ H &= \Delta\rho_1(\Delta\alpha_{24}+\Delta\alpha_{23}+\Delta\alpha_{34})+\Delta\rho_2(\Delta\alpha_{13}+\Delta\alpha_{14}+\Delta\alpha_{34})\\ &\quad+\Delta\rho_3(\Delta\alpha_{24}+\Delta\alpha_{14}+\Delta\alpha_{12})+\Delta\rho_4(\Delta\alpha_{13}+\Delta\alpha_{23}+\Delta\alpha_{12}),\\ I &= \Delta\rho_1(\Delta\alpha_{13}+\Delta\alpha_{14}+\Delta\alpha_{12})+\Delta\rho_2(\Delta\alpha_{24}+\Delta\alpha_{23}+\Delta\alpha_{12})\\ &\quad+\Delta\rho_3(\Delta\alpha_{13}+\Delta\alpha_{23}+\Delta\alpha_{34})\\ &\quad+\Delta\rho_4(\Delta\alpha_{24}+\Delta\alpha_{14}+\Delta\alpha_{34}),\\ A_1 &= \Delta\rho_1-\Delta\rho_2,\quad A_2=\Delta\rho_1+\Delta\rho_2,\quad A_3=\Delta\rho_3-\Delta\rho_4,\\ A_4 &= \Delta\rho_3+\Delta\rho_4,\qquad H_x=\Delta\alpha_{24}-\Delta\alpha_{13},\\ H_y &= \Delta\alpha_{23}-\Delta\alpha_{14},\quad H_z=\Delta\alpha_{34}-\Delta\alpha_{12}\end{aligned}\tag{A-6}$$

From Eq. (A-5), Raynes et al. obtained Eq. (8) in their paper for each of the f constants in terms of the F constants. This relationship should be applied to methane *in vacuo* or in gas. Thus internal coordinate force constant f can be obtained from the symmetry coordinate force constants F. However, hydrated methanes that we are analysing in this paper are subject to the asymmetrical potential field of surrounding water molecules. Thus the degeneracy of the modes *in vacuo* is resolved, and the four modes are separated into nine modes. The harmonic potential $V^{(2)}$ must be expressed in terms of symmetry coordinates instead of Eq. (A-4) as follows:

$$\begin{aligned}2V^{(2)} &= F_{11}S_1^2+(F_{22}^{(2a)}S_{2a}^2+F_{22}^{(2b)}S_{2b}^2)\\ &+(F_{33}^{(3x)}S_{3x}^2+F_{33}^{(3y)}S_{3y}^2+F_{33}^{(3z)}S_{3z}^2)\\ &+2(F_{34}^{(3x4x)}S_{3x}S_{4x}+F_{34}^{(3y4y)}S_{3y}S_{4y}+F_{34}^{(3z4z)}S_{3z}S_{4z})\\ &+(F_{44}^{(4x)}S_{4x}^2+F_{44}^{(4y)}S_{4y}^2+F_{44}^{(4z)}S_{4z}^2).\end{aligned}\tag{A-7}$$

Using Eqs. (A-3) and (A-6), we get the following from Eq. (A-7):

$$\begin{aligned}2V^{(2)} &= F_{11}\frac{1}{4}(A+2B)\\ &+F_{22}^{(2a)}\frac{1}{12}(C+3C_z-4D+6D_a+2E+6E_z)\\ &+F_{22}^{(2b)}\frac{1}{12}(3C-3C_z-6D_a+6E-6E_z)\\ &+F_{33}^{(3x)}\frac{1}{4}(A-2B+4B_x)+F_{33}^{(3y)}\frac{1}{4}(A-2B+4B_y)\\ &+F_{33}^{(3z)}\frac{1}{4}(A-2B+4B_z)+2F_{34}^{(3x4x)}\frac{1}{2\sqrt{2}}(A_1+A_3)H_x\\ &+2F_{34}^{(3y4y)}\frac{1}{2\sqrt{2}}(A_1-A_3)H_y+2F_{34}^{(3z4z)}\frac{1}{2\sqrt{2}}(A_2-A_4)H_z\\ &+F_{44}^{(4x)}\frac{1}{2}(C_x-2E_x)+F_{44}^{(4y)}\frac{1}{2}(C_y-2E_y)\\ &+F_{44}^{(4z)}\frac{1}{2}(C_z-2E_z).\end{aligned}\tag{A-8}$$

This equation demonstrates that the unique relationship between the f constants and the F constants that Raynes et al. obtained in their paper, does not exist. Hence we must not use their Eq. (8) in determining force constants of the harmonic potential energy. Alternatively, we use an allowable relationship. These are

$$\begin{aligned}F_{11} &= f_{rr}+3f_{rs},\quad F_{34}=\sqrt{2}(f_{rs}-f_{r\alpha}),\\ F_{22} &= f_{\alpha\alpha}-2f_{\alpha\beta}+f_{\alpha\omega},\quad F_{33}=f_{rr}-f_{rs},\\ F_{44} &= f_{\alpha\alpha}-f_{\alpha\omega}\end{aligned}\tag{A-9}$$

which are also given as Eq. (7) in their paper. With Eq. (A-9), we determined the force constants so as to produce correctly the experimental values of four vibrational frequencies using the GF method described in the following Appendix A.3.4. The force constants determined for methane are given in Table A2.

A.3. Normal mode analysis

A.3.1. Force constant matrix F of methane for internal motion

The hydrated methanes are influenced from the potential fields of the other methanes and of water molecules surrounding the methanes. Hence the total energy of the methanes in hydrate is described as $E_{\mathrm{m}}^{\mathrm{total}}=E_{\mathrm{met}}+E_{\mathrm{met-met}}+E_{\mathrm{met-wat}}$, which is part of Eq. (1). Consider one methane in the hydrate. Its potential energy V_{m} is expressed in terms of the second derivatives of the total energy $E_{\mathrm{m}}^{\mathrm{total}}$ with respect to internal variables ρ_i within the methane and internal coordinates $\Delta\rho_i$

(i = 1–10) as follows:

$$2V_{\mathrm{m}} = \sum_{i,j=1}^{10} \frac{\partial^2 E_{\mathrm{m}}^{\mathrm{total}}}{\partial\rho_i\partial\rho_j}\Delta\rho_i\Delta\rho_j = \sum_{i,j=1}^{10} \frac{\partial^2 \sum_{\mathrm{methanes}} V^{(2)}}{\partial\rho_i\partial\rho_j}\Delta\rho_i\Delta\rho_j + \sum_{i,j=1}^{10} \frac{\partial^2 \left(E_{\mathrm{m}}^{\mathrm{total}} - \sum_{\mathrm{methanes}} V^{(2)}\right)}{\partial\rho_i\partial\rho_j}\Delta\rho_i\Delta\rho_j = \sum_{i,j=1}^{10} f_{ij}\Delta\rho_i\Delta\rho_j + \sum_{i,j=1}^{10} \frac{\partial^2 \left(E_{\mathrm{m}}^{\mathrm{total}} - \sum_{\mathrm{methanes}} V^{(2)}\right)}{\partial\rho_i\partial\rho_j}\Delta\rho_i\Delta\rho_j = \sum_{i,j=1}^{10} F_{ij}\Delta\rho_i\Delta\rho_j \quad \text{(A-10)}$$

The constants f_{ij} are the internal coordinate force constants for the harmonic potential $V^{(2)}$ of Eq. (A-1). The elements F_{ij} of the force constant matrix F are comprised of the sum of contributions from the harmonic potential, the anharmonic potential and the other molecules' potential. The explicit expressions will be published elsewhere.

A.3.2. Kinetic energy matrix G of methane for internal motion

The kinetic energy T_{m} of a methane can be expressed in terms of the velocities of internal variable ρ_i or in terms of the momenta P_i, conjugate to the variables ρ_i. Then T_{m} is written as:

$$2T_{\mathrm{m}} = \sum_{i,j=1}^{10} G_{ij}P_iP_j$$

where the G_{ij} are coefficients involving the masses of the atoms and the geometry of methane. The elements G_{ij} of the kinetic energy matrix G are obtained as in Wilson's paper [17]:

$$g_{rr} = G_{\rho_i\rho_i} = \mu_0 + \mu_i$$

$$g_{rs} = G_{\rho_i\rho_j} = \mu_0 \cos\alpha_{ij}$$

$$g_{r\alpha} = G_{\rho_i\alpha_{ij}} = -\mu_0\tau_j \sin\alpha_{ij}$$

$$g_{r\beta} = G_{\rho_i\alpha_{jk}} = -\frac{\mu_0}{\sin\alpha_{jk}}\{\tau_j(\cos\alpha_{ik} - \cos\alpha_{jk}\cos\alpha_{ij}) + \tau_k(\cos\alpha_{ij} - \cos\alpha_{jk}\cos\alpha_{ik})\}$$

$$g_{\alpha\alpha} = G_{\alpha_{ij}\alpha_{ij}} = \mu_0\{\tau_i^2 + \tau_j^2 - 2\tau_i\tau_j\cos\alpha_{ij}\} + \mu_i\tau_i^2 + \mu_j\tau_j^2 \quad \text{(A-11)}$$

$$g_{\alpha\beta} = G_{\alpha_{ij}\alpha_{ik}} = \frac{\mu_0}{\sin\alpha_{ij}\sin\alpha_{ik}}(\tau_i - \tau_j\cos\alpha_{ij})(\tau_i - \tau_k\cos\alpha_{ik})(\cos\alpha_{jk} - \cos\alpha_{ij}\cos\alpha_{ik}) + \mu_0\tau_j\tau_k\sin\alpha_{ij}\sin\alpha_{ik} + \frac{\mu_i\tau_i^2}{\sin\alpha_{ij}\sin\alpha_{ik}}(\cos\alpha_{jk} - \cos\alpha_{ij}\cos\alpha_{ik})$$

$$g_{\alpha\varpi} = G_{\alpha_{ij}\alpha_{kh}} = \frac{\mu_0}{\sin\alpha_{ij}\sin\alpha_{kh}}\{(\tau_j - \tau_i\cos\alpha_{ij})(\tau_h - \tau_k\cos\alpha_{kh})\cos\alpha_{ik} + (\tau_j - \tau_i\cos\alpha_{ij})(\tau_k - \tau_h\cos\alpha_{kh})\cos\alpha_{ih} + (\tau_i - \tau_j\cos\alpha_{ij})(\tau_h - \tau_k\cos\alpha_{kh})\cos\alpha_{jk} + (\tau_i - \tau_j\cos\alpha_{ij})(\tau_k - \tau_h\cos\alpha_{kh})\cos\alpha_{jh}\}.$$

In Eq. (A-11), $\mu_0 = 1/m_{\mathrm{C}}$, $\mu_i = 1/m_{\mathrm{H}}$ (i = 1–4), $\tau_i = 1/\rho_i$ (i = 1–4). We also use the notation g_{rr} to express the elements $G_{\rho i\rho i}$ (i = 1–4) and so on.

A.3.3. Utilization of the symmetry coordinates

Because we are considering 10 internal variables ρ_i (i = 1–10), the matrices F and G have 10 × 10 elements, respectively. But there exists one relationship between 10 variables, so they are not all independent. Using the symmetry coordinates already introduced in Eq. (A-3), we can overcome this problem. Eq. (A-3) shows a transformation of internal coordinates to the symmetry coordinates. The transformation matrix U should be orthogonal. Then we add a symmetric redundant coordinate S_{R} to Eq. (A-3):

$$S_{\mathrm{R}} = \frac{1}{\sqrt{6}}(\Delta\alpha_{12} + \Delta\alpha_{13} + \Delta\alpha_{14} + \Delta\alpha_{23} + \Delta\alpha_{24} + \Delta\alpha_{34}).$$

Thus Eq. (A-3) is expressed in a form of a matrix product:

$$\boldsymbol{R}_{\mathrm{S}} = U\boldsymbol{R},$$

where

$$\tilde{\boldsymbol{R}}_{\mathrm{S}} = (S_1 S_R S_{2a} S_{2b} S_{3x} S_{4x} S_{3y} S_{4y} S_{3z} S_{4z})$$

$$\tilde{\boldsymbol{R}} = (\Delta\rho_1\Delta\rho_2\Delta\rho_3\Delta\rho_4\Delta\alpha_{12}\Delta\alpha_{13}\Delta\alpha_{14}\Delta\alpha_{34}\Delta\alpha_{24}\Delta\alpha_{23})$$

and $U^{-1} = \tilde{U}$; the tilde denotes the transposed matrix.

With the transformation matrix U, the potential energy V_{m} can be expressed as:

$$2V_{\mathrm{m}} = \tilde{\boldsymbol{R}}F\boldsymbol{R} = \tilde{\boldsymbol{R}}U^{-1}UFU^{-1}U\boldsymbol{R} = \tilde{\boldsymbol{R}}_{\mathrm{S}}F_{\mathrm{s}}\boldsymbol{R}_{\mathrm{S}}$$

where $F_{\mathrm{s}} = UF\tilde{U}$. The transformed force constant matrix F_{s} is a 10 × 10 matrix. Likewise, we can construct the transformed kinetic energy matrix $G_{\mathrm{s}} = UG\tilde{U}$, which has 10 × 10 elements. As shown by Raynes et al., the symmetry coordinate S_{R} depends on S_{2a}, S_{2b}, S_{4x}, S_{4y} and S_{4z}, and is zero at equilibrium. Therefore, we can drop the second row and the second column of the F_{s} and G_{s} matrices, which result from the calculation of the redundant coordinate S_{R}. Thus these matrices have 9 × 9 elements. Hereinafter, we will use the same notations F_{s} and G_{s} for the 9 × 9 matrices describing force constant and kinetic energy matrices. Realizing that the redundant coordinate S_{R} is unnecessary, the column vector $\boldsymbol{R}_{\mathrm{s}}$ has nine elements without S_{R}. Then the transformation matrix U becomes a 9 × 10 matrix, and the same notation U is used hereinafter.

A.3.4. GF method

Originally, with the matrices F and G, we have to solve the following eigenvalue equation $L^{-1}GFL = \Lambda$. This equation is changed to

$$\Lambda = L^{-1}U^{-1}UGU^{-1}UFU^{-1}UL = (UL)^{-1}UG\tilde{U}\,UF\tilde{U}\,UL,$$

where we use the original matrix U with S_R. Here we put $UL = L_s$. Then we have:

$$L_s^{-1}G_sF_sL_s = \Lambda \tag{A-12}$$

To do normal mode analysis, we have to solve this eigenvalue equation. Here the L_s and Λ are matrices comprised of the eigenvectors and eigenvalues of the matrix G_sF_s, respectively. Following Jacobi's method, we show the steps because certain matrices derived in the process of solving the equation are used in the following section.

First, we diagonalize the matrix G_s; $\tilde{A}G_sA = \Gamma$, where the A is orthogonal matrix, and the Γ is diagonal matrix. With the matrices A and Γ, we construct a matrix K: $K = \tilde{\Gamma}^{1/2}\tilde{A}F_sA\Gamma^{1/2}$. The matrix K is a symmetric matrix. Then diagonalizing the matrix K, we get the following: $\tilde{D}KD = \Lambda$, where the matrix Λ is the same eigenvalue matrix as in Eq. (A-12). The eigenvector matrix L_s in Eq. (A-12) is expressed as $L_s = A\Gamma^{1/2}D$. Thus we get the matrices L_s and Λ.

$$\Lambda = \begin{pmatrix} \lambda_1 & 0 & \cdots & 0 \\ 0 & \lambda_2 & \cdots & 0 \\ \cdots & & \cdots & \\ 0 & \cdots & 0 & \lambda_9 \end{pmatrix}$$

where $\lambda_1, \lambda_2, \ldots, \lambda_9$ are eigenvalues of the matrix G_sF_s. And $L_s = (\boldsymbol{l}_1, \boldsymbol{l}_2, \ldots, \boldsymbol{l}_9)$, where the column vector $\boldsymbol{l}_\alpha$ is the eigenvector belonging to the eigenvalue λ_α of the αth normal mode. With the normal mode coordinates $\boldsymbol{Q} = (Q_1, Q_2, \ldots, Q_9)$, the symmetry coordinates $\boldsymbol{R}_s$ are expressed as $\boldsymbol{R}_s = L_s\boldsymbol{Q}$. Thus the potential energy V_m is given in terms of normal mode coordinates as:

$$2V_m = \tilde{\boldsymbol{R}}_sF_s\boldsymbol{R}_s = \tilde{\boldsymbol{Q}}\tilde{L}_sF_sL_s\boldsymbol{Q} = \tilde{\boldsymbol{Q}}\tilde{D}\tilde{\Gamma}^{1/2}\tilde{A}F_sA\Gamma^{1/2}D\boldsymbol{Q}$$
$$= \tilde{\boldsymbol{Q}}\tilde{D}KD\boldsymbol{Q} = \tilde{\boldsymbol{Q}}\Lambda\boldsymbol{Q} = \sum_{\alpha=1}^{9}(\lambda_\alpha Q_\alpha^2).$$

A.4. Mean-square displacement matrix

A.4.1. Cartesian displacement coordinates and the normal mode coordinates

How do the normal mode coordinates $\boldsymbol{Q}$ excite five atoms in methane? To answer this, we introduce a transformation matrix L_X^s, which is a matrix relating Cartesian displacement coordinates $\Delta\boldsymbol{X}$ and the normal mode coordinates $\boldsymbol{Q}$, as follows:

$$\Delta\boldsymbol{X} = L_X^s\boldsymbol{Q} \tag{A-13}$$

The calculation of L_X^s is given in the following subsection.

A.4.2. Cartesian displacement coordinates and the internal coordinates

The internal coordinates $\mathbf{R}$ is related to the Cartesian displacement coordinates $\Delta\mathbf{X}$ via a transformation matrix B. Here we define several vectors necessary to construct the B matrix. The displacement vectors describing Cartesian displacement coordinates of carbon and hydrogens H_i ($i = 1, 4$) are denoted $\Delta\boldsymbol{r}_i$ ($i = 0$–4). A vector $\boldsymbol{e}_i$ is used as a unit vector pointing from carbon's position to the H_i's. Two unit vectors on the plane spanned by H_i, carbon and H_j are defined as $\mathbf{q}_{ij}$ and $-\mathbf{p}_{ij}$. The vectors $\boldsymbol{e}_j$ and $\boldsymbol{q}_{ij}$ are orthogonal, and the vectors $\boldsymbol{e}_i$ and $-\boldsymbol{p}_{ij}$ are orthogonal. Thus,

$$\boldsymbol{q}_{ij} = \frac{1}{\sin\alpha_{ij}}(\boldsymbol{e}_i - \cos\alpha_{ij}\boldsymbol{e}_j) \quad \text{and}$$
$$-\boldsymbol{p}_{ij} = \frac{1}{\sin\alpha_{ij}}(-\cos\alpha_{ij}\boldsymbol{e}_i + \boldsymbol{e}_j).$$

And we get following relationship:

$$\begin{pmatrix} \Delta\rho_1 \\ \Delta\rho_2 \\ \Delta\rho_3 \\ \Delta\rho_4 \\ \Delta\alpha_{12} \\ \Delta\alpha_{13} \\ \Delta\alpha_{14} \\ \Delta\alpha_{34} \\ \Delta\alpha_{24} \\ \Delta\alpha_{23} \end{pmatrix} = \begin{pmatrix} -\tilde{\boldsymbol{e}}_1 & \tilde{\boldsymbol{e}}_1 & \mathbf{0} & \mathbf{0} & \mathbf{0} \\ -\tilde{\boldsymbol{e}}_2 & \mathbf{0} & \tilde{\boldsymbol{e}}_2 & \mathbf{0} & \mathbf{0} \\ -\tilde{\boldsymbol{e}}_3 & \mathbf{0} & \mathbf{0} & \tilde{\boldsymbol{e}}_3 & \mathbf{0} \\ -\tilde{\boldsymbol{e}}_4 & \mathbf{0} & \mathbf{0} & \mathbf{0} & \tilde{\boldsymbol{e}}_4 \\ \frac{-\tilde{\boldsymbol{p}}_{12}}{\rho_1} + \frac{\tilde{\boldsymbol{q}}_{12}}{\rho_2} & \frac{\tilde{\boldsymbol{p}}_{12}}{\rho_1} & \frac{-\tilde{\boldsymbol{q}}_{12}}{\rho_2} & \mathbf{0} & \mathbf{0} \\ \frac{-\tilde{\boldsymbol{p}}_{13}}{\rho_1} + \frac{\tilde{\boldsymbol{q}}_{13}}{\rho_3} & \frac{\tilde{\boldsymbol{p}}_{13}}{\rho_1} & \mathbf{0} & \frac{-\tilde{\boldsymbol{q}}_{13}}{\rho_3} & \mathbf{0} \\ \frac{-\tilde{\boldsymbol{p}}_{14}}{\rho_1} + \frac{\tilde{\boldsymbol{q}}_{14}}{\rho_4} & \frac{\tilde{\boldsymbol{p}}_{14}}{\rho_1} & \mathbf{0} & \mathbf{0} & \frac{-\tilde{\boldsymbol{q}}_{14}}{\rho_4} \\ \frac{-\tilde{\boldsymbol{p}}_{34}}{\rho_3} + \frac{\tilde{\boldsymbol{q}}_{34}}{\rho_4} & \mathbf{0} & \mathbf{0} & \frac{\tilde{\boldsymbol{p}}_{34}}{\rho_3} & \frac{-\tilde{\boldsymbol{q}}_{34}}{\rho_4} \\ \frac{-\tilde{\boldsymbol{p}}_{42}}{\rho_4} + \frac{\tilde{\boldsymbol{q}}_{42}}{\rho_2} & \mathbf{0} & \frac{-\tilde{\boldsymbol{q}}_{42}}{\rho_2} & \mathbf{0} & \frac{\tilde{\boldsymbol{p}}_{42}}{\rho_4} \\ \frac{-\tilde{\boldsymbol{p}}_{23}}{\rho_2} + \frac{\tilde{\boldsymbol{q}}_{23}}{\rho_3} & \mathbf{0} & \frac{\tilde{\boldsymbol{p}}_{23}}{\rho_2} & \frac{-\tilde{\boldsymbol{q}}_{23}}{\rho_3} & \mathbf{0} \end{pmatrix} \times \begin{pmatrix} \Delta\boldsymbol{r}_0 \\ \Delta\boldsymbol{r}_1 \\ \Delta\boldsymbol{r}_2 \\ \Delta\boldsymbol{r}_3 \\ \Delta\boldsymbol{r}_4 \end{pmatrix}$$

where zero vector means a 1×3 row vector. That is, $\boldsymbol{R} = B\Delta\boldsymbol{X}$, where $\Delta\tilde{\boldsymbol{X}} = (\Delta\tilde{\boldsymbol{r}}_0\Delta\tilde{\boldsymbol{r}}_1\Delta\tilde{\boldsymbol{r}}_2\Delta\tilde{\boldsymbol{r}}_3\Delta\tilde{\boldsymbol{r}}_4)$.

By multiplying the transformation matrix U from the left hand side of $\boldsymbol{R} = B\Delta\boldsymbol{X}$, we obtain $\boldsymbol{R}_s = UB\Delta\boldsymbol{X} = B_s\Delta\boldsymbol{X}$, where $\boldsymbol{B}_s = UB$. With Eq. (A-13), we get a relationship $\boldsymbol{R}_s = B_s\Delta\boldsymbol{X} = B_sL_X^s\boldsymbol{Q}$. On the other hand, the symmetry coordinates $\boldsymbol{R}_s$ has the relation $\boldsymbol{R}_s = L_s\boldsymbol{Q}$. Thus we have $L_s = B_sL_X^s$.

In a different way using the transformation matrix B, the kinetic energy T_m is constructed as follows: $2T_m = \tilde{\boldsymbol{P}}BM^{-1}\tilde{B}\boldsymbol{P}$, where the matrix M is a 15×15 diagonal matrix whose elements are the masses of carbon and hydrogens (m_C, m_C, m_C, m_H, m_H, …, m_H). The matrix $BM^{-1}\tilde{B}$ must be the kinetic energy matrix G, which is given in Eq. (A-11). Comparing each element of the matrices, the proof is easily done. Thus we have $G_s = UG\tilde{U} = UBM^{-1}\tilde{B}\tilde{U} = B_sM^{-1}\tilde{B}_s$. Then

$G_s^{-1} = (\tilde{B}_s)^{-1} M B_s^{-1}$. The mass matrix M is $\tilde{B}_s G_s^{-1} B_s = M$. Thus we obtain a calculable form of the matrix L_X^s: $L_X^s = M^{-1} M L_X^s = M^{-1} \tilde{B}_s G_s^{-1} B_s L_X^s = M^{-1} \tilde{B}_s G_s^{-1} L_s$ This is what we want to obtain.

A.4.3. Anisotropic thermal vibration

We think it is helpful to show a concrete representation of anisotropic thermal vibrations of atoms in methane. First, we describe the elements of the $\Delta \boldsymbol{X} = L_X^s \boldsymbol{Q}$ as follows:

$$\begin{pmatrix} \Delta x_0 \\ \Delta y_0 \\ \Delta z_0 \\ \Delta x_1 \\ \Delta y_1 \\ \Delta z_1 \\ \vdots \\ \Delta x_4 \\ \Delta y_4 \\ \Delta z_4 \end{pmatrix} = \begin{pmatrix} l_{0x1} & l_{0x2} & \cdots & l_{0x8} & l_{0x9} \\ l_{0y1} & l_{0y2} & \cdots & l_{0y8} & l_{0y9} \\ l_{0z1} & l_{0z2} & \cdots & l_{0z8} & l_{0z9} \\ l_{1x1} & l_{1x2} & \cdots & l_{1x8} & l_{1x9} \\ l_{1y1} & l_{1y2} & \cdots & l_{1y8} & l_{1y9} \\ l_{1z1} & l_{1z2} & \cdots & l_{1z8} & l_{1z9} \\ \vdots & \vdots & \cdots & \vdots & \vdots \\ l_{4x1} & l_{4x2} & \cdots & l_{4x8} & l_{4x9} \\ l_{4y1} & l_{4y2} & \cdots & l_{4y8} & l_{4y9} \\ l_{4z1} & l_{4z2} & \cdots & l_{4z8} & l_{4z9} \end{pmatrix} \begin{pmatrix} Q_1 \\ Q_2 \\ \vdots \\ Q_8 \\ Q_9 \end{pmatrix} \quad \text{(A-14)}$$

Here the displacement coordinate of carbon is $\Delta \tilde{\boldsymbol{r}}_0 = (\Delta x_0 \Delta y_0 \Delta z_0)$, and those of hydrogen H_i are $\Delta \tilde{\boldsymbol{r}}_i = (\Delta x_i \Delta y_i \Delta z_i)$ (i = 1–4). The element $l_{ij\alpha}$ of the matrix L_X^s has three subscripts: the first specifies atoms, the second the coordinate component, and the third the αth normal mode. For example, the x-component of displacement of carbon due to the αth normal mode is $\Delta x_0^\alpha = l_{0x\alpha} Q_\alpha$. The root-mean-square amplitude $\langle Q_\alpha^2 \rangle^{1/2}$ of thermal fluctuations of the normal mode coordinate Q_α is given by:

$$\sqrt{\langle Q_\alpha^2 \rangle} = \sqrt{\frac{k_B T}{\lambda_\alpha}},$$

where k_B is the Boltzmann constant and T is the absolute temperature. Next, an anisotropic thermal fluctuations of the xy component of displacement of carbon is given as follows:

$$\langle \Delta x_0 \Delta y_0 \rangle = \left\langle \sum_{\alpha=1}^{9} l_{0x\alpha} Q_\alpha \sum_{\beta=1}^{9} l_{0y\beta} Q_\beta \right\rangle = \sum_{\alpha=1}^{9} \sum_{\beta=1}^{9} l_{0x\alpha} l_{0y\beta} \langle Q_\alpha Q_\beta \rangle$$

$$= \sum_{\alpha=1}^{9} \sum_{\beta=1}^{9} l_{0x\alpha} l_{0y\beta} \frac{k_B T}{\lambda_\alpha} \delta_{\alpha\beta} = \sum_{\alpha=1}^{9} l_{0x\alpha} l_{0y\alpha} \frac{k_B T}{\lambda_\alpha}$$

Thus the mean-square displacement matrix of the carbon caused by normal modes excited thermally at temperature T is given by:

$$\begin{pmatrix} \langle \Delta x_0 \Delta x_0 \rangle & \langle \Delta x_0 \Delta y_0 \rangle & \langle \Delta x_0 \Delta z_0 \rangle \\ \langle \Delta y_0 \Delta x_0 \rangle & \langle \Delta y_0 \Delta y_0 \rangle & \langle \Delta y_0 \Delta z_0 \rangle \\ \langle \Delta z_0 \Delta x_0 \rangle & \langle \Delta z_0 \Delta y_0 \rangle & \langle \Delta z_0 \Delta z_0 \rangle \end{pmatrix} \quad \text{(A-15)}$$

References

[1] E.D. Sloan Jr., Clathrate Hydrates of Natural Gases, 2nd ed., Marcel Dekker Inc., New York, 1998 (revised and expanded).

[2] R.K. McMullan, G.A. Jeffrey, Polyhedral clathrate hydrates. IX. Structure of ethylene oxide hydrate, J. Chem. Phys. 42 (1965) 2725–2732.

[3] T.C.W. Mak, R.K. McMullan, Polyhedral clathrate hydrates. X. structure of the double hydrate of tetrahydrofuran and hydrogen sulfide, J. Chem. Phys. 42 (1965) 2732–2737.

[4] I.-M. Chou, A. Sharma, R.C. Burruss, J. Shu, H. Mao, R.J. Hemley, A.F. Goncharov, L.A. Stern, S.H. Kirby, Transformations in methane hydrates, Proc. Natl. Acad. Sci. U.S.A. 97 (2000) 13484–13487.

[5] A.K. Sum, R.C. Burruss, E.D. Sloan Jr., Measurement of clathrate hydrates via Raman spectroscopy, J. Phys. Chem. B 101 (1997) 7371–7377.

[6] T. Uchida, R. Okabe, K. Gohara, S. Mae, Y. Seo, H. Lee, S. Takeya, J. Nagao, T. Ebinuma, H. Naria, Raman spectroscopic observations of methane-hydrate formation and hydrophobic hydration around methane molecules in solution, Can. J. Phys. 81 (2003) 359–366.

[7] S. Yoshioki, Dynamics of a protein and water molecules surrounding the protein: hydrogen-bonding between vibrating water molecules and a fluctuating protein, J. Comput. Chem. 23 (2002) 402–413.

[8] S. Yoshioki, Application of the independent molecule model to the calculation of free energy and rigid-body motions of water hexamers, J. Mol. Graph. Model. 21 (2003) 487–498.

[9] S. Yoshioki, Application of the independent molecule model to the calculation of free energy and rigid-body motions of water heptamers and octamers, J. Mol. Graph. Model. 23 (2004) 111–127.

[10] W.T. Raynes, P. Lazzeretti, R. Zanasi, A.J. Sadlej, P.W. Fowler, Calculations of the force field of the methane molecule, Mol. Phys. 60 (1987) 509–525.

[11] T. Nishikawa (Ed.), Physics Dictionary, Baifukan, Tokyo, 1984 , p. 2362 (in Japanese).

[12] F.A. Momany, L.M. Carruthers, R.F. McGuire, H.A. Scheraga, Intermolecular potential from crystal data. III. Determination of empirical potentials and application to the packing configurations and lattice energies in crystals of hydrocarbon, carboxylic acids, amine, and amides, J. Phys. Chem. 78 (1974) 1595–1620.

[13] S. Yoshioki, Formulation of the Hessian matrix for the conformational energy of protein–water systems, J. Phys. Soc. Jpn. 66 (1997) 2927–2935.

[14] S. Yoshioki, to be prepared.

[15] P.E. Gill, W. Murray, M.H. Wright, Practical Optimization, Academic Press, London, 1981, p. 105.

[16] E.B. Wilson Jr., A method of obtaining the expanded secular equation for the vibration frequencies of a molecule, J. Chem. Phys. 7 (1939) 1047–1052.

[17] E.B. Wilson Jr., Some mathematical methods for the study of molecular vibrations, J. Chem. Phys. 9 (1941) 76–84.

[18] E.B. Wilson Jr., J.C. Decius, P.C. Cross, Molecular Vibrations, McGraw-Hill Book Company Inc., New York, 1955, p. 117.

[19] C.K. Johnson, ORTEP: A Fortran Thermal Ellipsoid Plot Program, ORNL-3795, Oak Ridge National Laboratory, Oak Ridge, Tennessee, USA, 1965

[20] S. Yoshioki, Motions of water molecules surrounding a rigid protein model, J. Phys. Soc. Jpn. 67 (1998) 1477–1485.

[21] J.A. Greathouse, R.T. Cygan, B.A. Simmons, Vibrational spectra of methane clathrates from molecular dynamics simulation, J. Phys. Chem. B 110 (2006) 6428–6431.

[22] J.S. Tse, Vibrations of methane in structure I clathrate hydrate—An ab initio density functional molecular dynamics study, J. Supramol. Chem. 2 (2002) 429–433.

[23] H. Itoh, K. Kawamura, Molecular dynamics simulations of clathrate hydrate, Ann. NY Acad. Sci. 912 (2000) 693–701.

[24] D.L. Gray, A.G. Robiette, The anharmonic force field and equilibrium structure of methane, Mol. Phys. 37 (1979) 1901–1920.